








Band-edge absorption characteristics of semi-insulating indium phosphide under unified Franz-Keldysh and Einstein models

Alexander C. MacGillivray ^{1,*},† Nikolai I. Lesack ^{1,*} Ilija R. Hristovski ¹ Matthias F. Jenne ¹ Benjamin C. Maglio ²
 Sayra Gorgani ¹ and Jonathan F. Holzman^{1,‡}

¹*School of Engineering, The University of British Columbia, 1137 Alumni Avenue, Kelowna, British Columbia, Canada V1V 1V7*

²*School of Physics and Astronomy, Cardiff University, The Parade, Cardiff CF24 3AA, United Kingdom*

 (Received 6 September 2021; revised 1 February 2022; accepted 23 March 2022; published 6 April 2022)

The foundational Franz-Keldysh effect and Einstein model are applied in this work to characterize semiconductor band-edge absorption—and its departures from ideality. We unify the Franz-Keldysh and Einstein models to fully characterize the field-induced tunneling of photoexcited electrons from degenerate valence bands into the conduction band, with encroachment into the band gap arising as an Urbach tail. Our unified model is implemented for semi-insulating indium phosphide (SI-InP) with strong agreement seen between the theoretical and experimental results for varied photon energies and electric fields.

DOI: [10.1103/PhysRevB.105.155203](https://doi.org/10.1103/PhysRevB.105.155203)

I. INTRODUCTION

Semiconductor physics and devices have evolved over the past century, with much of the interest owing to their enabling of interactions with light and fields. The understanding of such interactions reached a milestone in 1958 via formulations by Franz [1] and Keldysh [2]. The Franz-Keldysh effect proposed that an electric field could constrict a band gap to promote tunneling of photoexcited electrons from the valence to conduction band. This would give increased absorption at photon energies below the band-gap energy [3,4]. The Franz-Keldysh effect was later demonstrated and applied via electrorefraction, spanning the work of Seraphin and Bottka [5] to Pintus *et al.* [6], or electroabsorption, spanning the work of Chester and Wendland [7] to ourselves [8].

Nonetheless, challenges remain in interpreting and applying the underlying Franz-Keldysh model. The past [7,9] and present [10] literature show a complex interplay between photon energy, temperature, and electric field—with assumptions yielding potentially significant departures from ideality. The challenges arise here because the ideal band gap neglects the continuum of Urbach tail states that can arise at the band edges. These states encroach into the band gap and yield field-induced changes in absorption that are especially strong (in comparison to those predicted in an ideal band gap) [8,11] and temperature dependent (as thermal energy transforms the characteristics of the Urbach tail) [12,13].

In this work, we unite the Franz-Keldysh model, with degeneracy in the valence band and Urbach tails in the valence and conduction bands, to the Einstein model, characterizing the temperature dependence of the tail states. The theoretical results for our unified Franz-Keldysh and Einstein

models are compared to experimental results for semi-insulating indium phosphide (SI-InP) under varied photon energies, temperatures, and electric fields. Strong agreement is seen—suggesting that the unified model can give deeper understanding on the interactions of light and field in semiconductors. Such knowledge can support the development of electroabsorption modulators operating with standard laser wavelengths, such as 980 nm, and nonepitaxial semiconductors, such as SI-InP.

II. THEORETICAL MODELS

The following subsections detail the Einstein model, Franz-Keldysh model, and our proposed unified Franz-Keldysh and Einstein model.

A. Einstein model

The Einstein model characterizes the continuum of states at the band edge of a semiconductor. The states encroach into the band gap in the form of an Urbach tail with its band gap and characteristic width having energies of [13]

$$E_g(T) = E_{g,0} - S_g k_B \theta_E \frac{1}{\exp(\theta_E/T) - 1} \quad (1)$$

and

$$E_0(T) = S_0 k_B \theta_E \left(\frac{1 + X}{2} + \frac{1}{\exp(\theta_E/T) - 1} \right), \quad (2)$$

respectively, where k_B is Boltzmann's constant, and T is the temperature. The material parameters are defined for the material of interest to this work, SI-InP, in accordance with the findings of Beaudoin *et al.* [13]: $E_{g,0} = 1.4236$ eV is the band-gap energy at 0 K, $\theta_E = 316.5$ K is three-quarters of the Debye temperature; $S_0 = 0.173$ is a dimensionless constant linked to electron-phonon coupling; $S_g = 5.12$ is a

*These authors contributed equally to this work.

†alex.macgillivray@ubc.ca

‡jonathan.holzman@ubc.ca

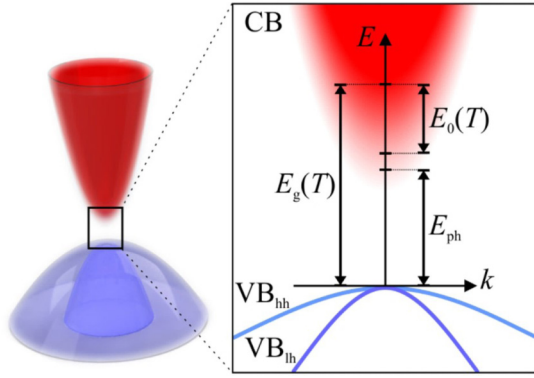


FIG. 1. The central Γ valley of SI-InP as energy E versus wave vector k . The inset shows the band structure with a degenerate valence band, for heavy (VB_{hh}) and light (VB_{lh}) holes, an Urbach tail in the conduction band (CB), with states decaying down from $E_g(T)$ over a characteristic width of $E_0(T)$, and a photon energy of E_{ph} .

dimensionless coupling constant; $X = 1.1$ is a dimensionless constant characterizing structural disorder. The central Γ -valley of SI-InP is depicted in Fig. 1 as energy E versus wave vector k with the band structure detailed in the inset. The inset shows degeneracy in the valence band, as heavy- and light-hole bands, an Urbach tail in the conduction band, as states encroaching into $E_g(T)$ over a characteristic width of $E_0(T)$, and a photon energy of E_{ph} . For expository purposes, this figure and the remainder of this work depict the encroachment at the conduction band with sharp edges at the valence band, as seen elsewhere [14]. However, it should be understood that the absorption characteristics manifest via a joint density of states distribution for electron transitions from a tail of encroaching states at the degenerate valence bands to a tail of encroaching states at the conduction band.

B. Franz-Keldysh model

The Franz-Keldysh model manifests as an electric-field-induced perturbation to the absorption of a semiconductor. It is characterized in this work by the fundamental theories of Franz [1] and Keldysh [2] and extensions by Bennett and Soref [3]. Their theory quantifies field-induced tunneling of photoexcited electrons from valence bands to an idealized conduction band, which can be visualized in Fig. 1 as a perfect curve with $E_0(T) = 0$ and a well-defined minimum at $E_g(T)$. In this work, according to the depiction above, we expand

the theory to have a continuum of states in the conduction band, distributed over a generalized energy E , with the states decaying from the conduction band edge at $E_g(T)$ over a characteristic width of $E_0(T)$ in accordance with the Einstein model. This is illustrated in Fig. 1. A gradient is formed in this conduction band when a uniform electric field \mathcal{E} is applied, which aids tunneling of electrons from the valence to conduction band. This perturbs the real component ε_1 and imaginary component ε_2 of the complex dielectric constant, $\varepsilon = \varepsilon_1 + i\varepsilon_2$, which manifest as [3]

$$\begin{aligned} \Delta\varepsilon_{1,i}(E_{\text{ph}}, \mathcal{E}) &= a_1 \frac{\hbar^2(1+m_0/m_i)\mu_{e-i}^{3/2}}{E_{\text{ph}}^2} \omega_{\mathcal{E},i}^{1/2} \\ &\times \left[\pi \text{Ai}'\left(\frac{E-E_{\text{ph}}}{\hbar\omega_{\mathcal{E},i}}\right) \text{Bi}'\left(\frac{E-E_{\text{ph}}}{\hbar\omega_{\mathcal{E},i}}\right) \right. \\ &- \pi \left(\frac{E-E_{\text{ph}}}{\hbar\omega_{\mathcal{E},i}}\right) \text{Ai}\left(\frac{E-E_{\text{ph}}}{\hbar\omega_{\mathcal{E},i}}\right) \text{Bi}\left(\frac{E-E_{\text{ph}}}{\hbar\omega_{\mathcal{E},i}}\right) \\ &\left. + \left(\frac{E-E_{\text{ph}}}{\hbar\omega_{\mathcal{E},i}}\right)^{1/2} \text{u}\left(\frac{E-E_{\text{ph}}}{\hbar\omega_{\mathcal{E},i}}\right) \right] \quad (3a) \end{aligned}$$

and

$$\begin{aligned} \Delta\varepsilon_{2,i}(E_{\text{ph}}, \mathcal{E}) &= a_1 \frac{\hbar^2(1+m_0/m_i)\mu_{e-i}^{3/2}}{E_{\text{ph}}^2} \omega_{\mathcal{E},i}^{1/2} \left[\pi \text{Ai}'^2\left(\frac{E-E_{\text{ph}}}{\hbar\omega_{\mathcal{E},i}}\right) \right. \\ &- \pi \left(\frac{E-E_{\text{ph}}}{\hbar\omega_{\mathcal{E},i}}\right) \text{Ai}^2\left(\frac{E-E_{\text{ph}}}{\hbar\omega_{\mathcal{E},i}}\right) \\ &\left. - \left(-\frac{E-E_{\text{ph}}}{\hbar\omega_{\mathcal{E},i}}\right)^{1/2} \text{u}\left(-\frac{E-E_{\text{ph}}}{\hbar\omega_{\mathcal{E},i}}\right) \right], \quad (3b) \end{aligned}$$

respectively. Here, a_1 is a material-dependent constant and $\omega_{\mathcal{E},i} = [e^2\mathcal{E}^2/(2\hbar m_{e-i})]^{1/3}$ is an angular frequency characterizing field-induced perturbation, where e is the electron charge and \hbar is the reduced Planck's constant. The subscript i instantiates heavy-hole ($i = \text{hh}$) and light-hole ($i = \text{lh}$) contributions, such that $\mu_{e-\text{hh}}$ and $\mu_{e-\text{lh}}$ are reduced effective masses of the electron with heavy and light holes, respectively, and m_0 , m_{hh} , and m_{lh} are effective masses of the free electron, heavy hole, and light hole, respectively. The expressions are stated in terms of the Heaviside function, $\text{u}(\cdot)$, Airy function, $\text{Ai}(\cdot)$, and Bairy function, $\text{Bi}(\cdot)$, where a primed symbol denotes differentiation of the function with respect to its argument. Given the definition of the absorption coefficient, $2E_{\text{ph}}\varepsilon_2/(2\hbar cn)$, and $\Delta\varepsilon_{2,i}(E_{\text{ph}}, \mathcal{E})$ from Eq. (4), the field-induced change in absorption coefficient for each $i = \text{hh}$ and lh can be expressed as [3]

$$\begin{aligned} \Delta\alpha_i(E, E_{\text{ph}}, \mathcal{E}) &= \frac{2E_{\text{ph}}\Delta\varepsilon_{2,i}(E_{\text{ph}}, \mathcal{E})}{2\hbar cn} = a_1 \frac{\hbar(1+m_0/m_i)\mu_{e-i}^{3/2}}{cnE_{\text{ph}}} \omega_{\mathcal{E},i}^{1/2} \\ &\times \left[\pi \text{Ai}'^2\left(\frac{E-E_{\text{ph}}}{\hbar\omega_{\mathcal{E},i}}\right) - \pi \left(\frac{E-E_{\text{ph}}}{\hbar\omega_{\mathcal{E},i}}\right) \text{Ai}^2\left(\frac{E-E_{\text{ph}}}{\hbar\omega_{\mathcal{E},i}}\right) - \left(-\frac{E-E_{\text{ph}}}{\hbar\omega_{\mathcal{E},i}}\right)^{1/2} \text{u}\left(-\frac{E-E_{\text{ph}}}{\hbar\omega_{\mathcal{E},i}}\right) \right], \quad (4) \end{aligned}$$

where c is the free-space speed of light and $n = \varepsilon_1^{1/2}$ is the refractive index. Here, the first two terms in brackets become zero as the applied electric field approaches zero, which leaves the third term with the expected square-root dependence on $E_{\text{ph}} - E$ if

(and only if) E_{ph} exceeds E . The absorption coefficient for each $i = \text{hh}$ and lh can then be cast as [3]

$$\alpha_i(E, E_{\text{ph}}, \mathcal{E}) = a_1 \frac{\hbar\pi(1 + m_0/m_i)\mu_{e-i}^{3/2}}{cnE_{\text{ph}}} \omega_{\mathcal{E},i}^{1/2} \left[\text{Ai}'^2\left(\frac{E - E_{\text{ph}}}{\hbar\omega_{\mathcal{E},i}}\right) - \left(\frac{E - E_{\text{ph}}}{\hbar\omega_{\mathcal{E},i}}\right) \text{Ai}^2\left(\frac{E - E_{\text{ph}}}{\hbar\omega_{\mathcal{E},i}}\right) \right]. \quad (5)$$

C. Unified Franz-Keldysh and Einstein model

We now unify the Franz-Keldysh and Einstein models to define the absorption coefficient of a semiconductor for field-induced transitions from degenerate valence bands to the conduction band, with states distributed in a continuum. For this, we integrate E over a product of $\alpha_i(E_{\text{ph}}, T, \mathcal{E})$, in Eq. (5), and a weighting distribution of $\exp[-(E_{\text{g}}(T) - E)/E_0(T)]$, according to the characteristics of $E_{\text{g}}(T)$ and $E_0(T)$ in Eqs. (1) and (2), respectively. This gives a total absorption coefficient, summed over heavy and light hole contributions, of

$$\begin{aligned} \alpha(E_{\text{ph}}, T, \mathcal{E}) &= a_2 \sum_{i=\text{hh},\text{lh}} \int_{E_{\text{ph}} - \delta_{\text{VB}}}^{E_{\text{g}}(T) + \delta_{\text{CB}}} \alpha_i(E, E_{\text{ph}}, \mathcal{E}) \exp\left(-\frac{E_{\text{g}}(T) - E}{E_0(T)}\right) dE \\ &= a_0 \sum_{i=\text{hh},\text{lh}} \int_{E_{\text{ph}} - \delta_{\text{VB}}}^{E_{\text{g}}(T) + \delta_{\text{CB}}} (1 + m_0/m_i) \frac{\mu_{e-i}^{3/2} \omega_{\mathcal{E},i}^{1/2}}{\hbar E_{\text{ph}}} \exp\left(-\frac{E_{\text{g}}(T) - E}{E_0(T)}\right) \\ &\quad \times \left[\text{Ai}'^2\left(\frac{E - E_{\text{ph}}}{\hbar\omega_{\mathcal{E},i}}\right) - \left(\frac{E - E_{\text{ph}}}{\hbar\omega_{\mathcal{E},i}}\right) \text{Ai}^2\left(\frac{E - E_{\text{ph}}}{\hbar\omega_{\mathcal{E},i}}\right) \right] dE, \end{aligned} \quad (6)$$

where a_2 is a normalization factor arising from the weighting, $a_0 = a_1 a_2 \hbar^2 \pi / (nc)$ is a constant, being roughly temperature independent in this work, and the parameters δ_{CB} and δ_{VB} are included in the integral limits for expository purposes, as detailed below. For a closed-form solution, we substitute $z_i = (E - E_{\text{ph}})/(\hbar\omega_{\mathcal{E},i})$ into Eq. (5) and the result into Eq. (6) to give

$$\begin{aligned} \alpha(E_{\text{ph}}, T, \mathcal{E}) &= a_0 \sum_{i=\text{hh},\text{lh}} \frac{(1 + m_0/m_i)\mu_{e-i}^{3/2} \omega_{\mathcal{E},i}^{3/2}}{E_{\text{ph}}} \int_{-\delta_{\text{VB}}/(\hbar\omega_{\mathcal{E},i})}^{(E_{\text{g}}(T) + \delta_{\text{CB}} - E_{\text{ph}})/(\hbar\omega_{\mathcal{E},i})} (\text{Ai}'^2(z_i) - z_i \text{Ai}^2(z_i)) \exp\left(-\frac{E_{\text{g}}(T) - \hbar\omega_{\mathcal{E},i} z_i - E_{\text{ph}}}{E_0(T)}\right) dz_i \\ &= a_0 \exp\left(-\frac{E_{\text{g}}(T) - E_{\text{ph}}}{E_0(T)}\right) \sum_{i=\text{hh},\text{lh}} \frac{(1 + m_0/m_i)\mu_{e-i}^{3/2} \omega_{\mathcal{E},i}^{3/2}}{E_{\text{ph}}} \int_{-\delta_{\text{VB}}/(\hbar\omega_{\mathcal{E},i})}^{(E_{\text{g}}(T) + \delta_{\text{CB}} - E_{\text{ph}})/(\hbar\omega_{\mathcal{E},i})} (\text{Ai}'^2(z_i) - z_i \text{Ai}^2(z_i)) \exp\left(\frac{\hbar\omega_{\mathcal{E},i} z_i}{E_0(T)}\right) dz_i \\ &= a_0 \exp\left(-\frac{E_{\text{g}}(T) - E_{\text{ph}}}{E_0(T)}\right) \sum_{i=\text{hh},\text{lh}} \frac{(1 + m_0/m_i)\mu_{e-i}^{3/2} \omega_{\mathcal{E},i}^{3/2}}{E_{\text{ph}}} \times \sum_{j=0}^{\infty} \left(\frac{\hbar\omega_{\mathcal{E},i}}{E_0(T)}\right)^j \frac{1}{j!} [H_j\{[E_{\text{g}}(T) + \delta_{\text{CB}} - E_{\text{ph}}]/(\hbar\omega_{\mathcal{E},i})\} \\ &\quad - I_{j+1}\{[E_{\text{g}}(T) + \delta_{\text{CB}} - E_{\text{ph}}]/(\hbar\omega_{\mathcal{E},i})\} - H_j[-\delta_{\text{VB}}/(\hbar\omega_{\mathcal{E},i})] + I_{j+1}[-\delta_{\text{VB}}/(\hbar\omega_{\mathcal{E},i})]], \end{aligned} \quad (7)$$

where a Taylor series expansion was applied to the exponential function in the integrand of the second expression to form the final expression. In general, the absorption coefficient can be computed via numerical integration, using Eq. (6), or closed-form computation, using Eq. (7) and the recursion relations for the functions $H_j(\cdot)$ and $I_j(\cdot)$ in the Appendix. Theoretically, the contributions from all states would be summed by driving the upper limit to infinity, via $\delta_{\text{CB}} \rightarrow \infty$, and the lower limit to zero, via $\delta_{\text{VB}} = E_{\text{ph}}$. In reality, however, the limits can be truncated by making δ_{CB} and δ_{VB} only sufficiently large to have further increases yield negligible contributions to the result. Our validations of Eqs. (6) and (7) suggest that δ_{CB} can be as low as zero, when the conduction band edge and photon energy are well separated, i.e., $E_{\text{g}}(T) - E_{\text{ph}} \gg E_0(T)$, as the absorption coefficient here is dominated by the Urbach tail states below $E_{\text{g}}(T)$. In addition, δ_{VB} should be kept well less than E_{ph} , to avoid integrating over states near the valence band. These lower states contribute little to the result, but they can be a concern in computing the closed-form expression in Eq. (7). They yield extremely large values for the Airy functions, which must be dampened by an equally strong and well-resolved exponential function, and

this can only be done by including many terms in its expansion (with j potentially spanning into the hundreds).

III. EXPERIMENT

Measurements were carried out on the field-induced changes in absorption coefficient for an iron-doped SI-InP sample having a resistivity of $10^8 \Omega \text{ cm}$, an orientation of (100), a thickness of $600 \mu\text{m}$, and a refractive index of $n = 3.4$. The SI-InP sample was mounted between two 175-nm-thick indium tin oxide (ITO) films, on polyethylene terephthalate (PET) substrates, onto which voltages were applied to establish the electric field. This left a thin air gap between the ITO and SI-InP. The absorption coefficient was extracted from measurements of power through this system at a photon energy of E_{ph} , a temperature of T , and an applied electric field of \mathcal{E} . Given an incident power on the air-SI-InP interface of $P_i(E_{\text{ph}}, T, \mathcal{E})$ and a transmitted power out of the SI-InP-air interface of $P_t(E_{\text{ph}}, T, \mathcal{E})$, the absorption coefficient was computed from $\alpha(E_{\text{ph}}, T, \mathcal{E}) = -\ln\{P_t(E_{\text{ph}}, T, \mathcal{E})/[P_i(E_{\text{ph}}, T, \mathcal{E})(1-R)^2]\}/d$, where $R = (n-1)^2/(n+1)^2$ is the reflectivity and

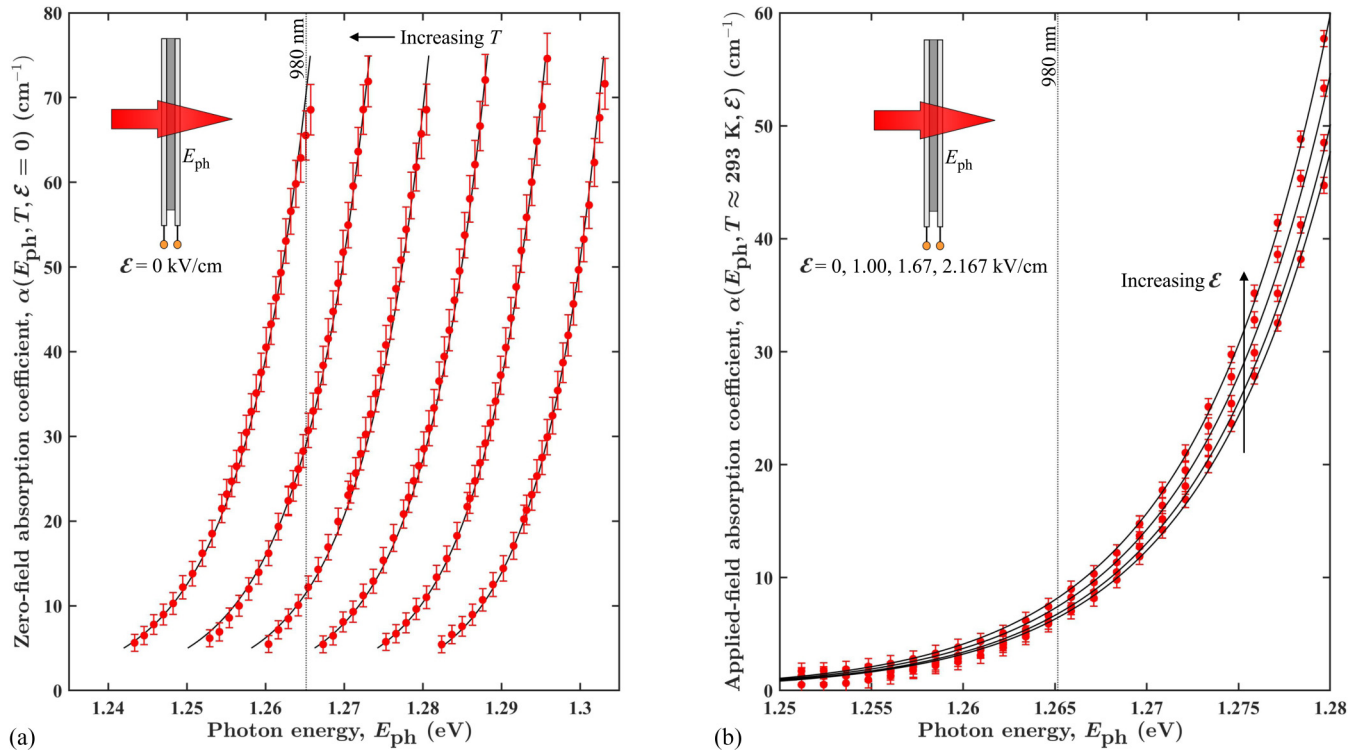


FIG. 2. The (a) zero-field absorption coefficient of SI-InP, $\alpha(E_{\text{ph}}, T, \mathcal{E} = 0 \text{ kV/cm})$, as a function of photon energy E_{ph} at a temperature of T and an applied electric field of $\mathcal{E} = 0 \text{ kV/cm}$, and the (b) applied-field absorption coefficient of SI-InP, $\alpha(E_{\text{ph}}, T \approx 293 \text{ K}, \mathcal{E})$, as a function of photon energy E_{ph} at room temperature, $T \approx 293 \text{ K}$, and an applied electric field of \mathcal{E} . In (a), curves from right to left correspond to incremented temperatures in steps of 15 K, with results displayed as experimental (red) markers and fitted theoretical (black) curves. In (b), curves from bottom to top correspond to electric fields of $\mathcal{E} = 0, 1.00, 1.67, \text{ and } 2.17 \text{ kV/cm}$, with results displayed as experimental (red) markers and fitted theoretical (black) curves. The photon energy for 980 nm radiation is marked by a dotted vertical line.

$d = 600 \mu\text{m}$ is the thickness. Such an expression is valid given that cascaded internal reflections, i.e., etalon effects, only lessen the transmitted power by a few percent, e.g., less than 4% at 980 nm. The temperature and electric field were varied by a heat source and DC voltage source (Stanford Research Systems, PS350), respectively, while the temperature was monitored by a thermal camera (FLIR ONE Pro). The above measurements were made versus photon energy by a spectrometer (Thorlabs, CCS200) with a broadband light source, and at a single photon energy with a 980-nm laser diode module (Newport, LQD980-220E) operating at 5 mW, silicon photodiode (Thorlabs, DET36A/M), and preamplifier (Stanford Research Systems, SR570).

IV. RESULTS

Results are shown in this section for the absorption coefficient versus photon energy, temperature, and electric field. Figure 2(a) shows results for the zero-field absorption coefficient of SI-InP, $\alpha(E_{\text{ph}}, T, \mathcal{E} = 0 \text{ kV/cm})$, as a function of photon energy, E_{ph} , spanning 1.24 to 1.30 eV, at a temperature of T and an applied electric field of $\mathcal{E} = 0 \text{ kV/cm}$. The curves correspond to temperatures increasing in 15-K steps from right to left, with experimental (red) markers and fitted theoretical (black) curves from the unified Franz-Keldysh and Einstein model. The absorption coefficients in the displayed range rise for increasing photon energy and / or temperature,

as expected, with good agreement between the experimental and theoretical results. Absorption coefficients below and above this range grow exceedingly small and large, respectively, yielding increased systematic error (not shown) and random error (shown by error bars), respectively.

Figure 2(b) shows results for the applied-field absorption coefficient of SI-InP, $\alpha(E_{\text{ph}}, T \approx 293 \text{ K}, \mathcal{E})$, as a function of photon energy E_{ph} spanning 1.25–1.28 eV, at room temperature, $T \approx 293 \text{ K}$, and an applied electric field of \mathcal{E} . The curves from bottom to top correspond to applied electric fields of $\mathcal{E} = 0, 1.00, 1.67, \text{ and } 2.17 \text{ kV/cm}$, with experimental (red) markers and fitted theoretical (black) curves. Overall, we see the absorption coefficient rise for increasing photon energy and / or applied electric field, as expected, with good agreement between the experimental and theoretical results. These best-fit curves are generated with the established parameters of SI-InP, listed earlier, and the multiplicative constant of $a_0 = 1.28 \times 10^{16} \text{ J s}^{3/2}/(\text{m kg}^{3/2})$ as the sole fitting parameter. (The fitting uses $\delta_{\text{CB}} = 1.35 \text{ eV}$ and $\delta_{\text{VB}} = 1.34 \text{ eV}$, but larger values can be used for these parameters with negligible change to the theoretical results). At the extremes of low and high photon energies, the results show weak and strong field-induced changes in absorption coefficient, respectively, as the separations between the photon energies and band-gap energy, $E_g(T \approx 293 \text{ K}) = 1.352 \text{ eV}$, are large and small, respectively. At an intermediate photon energy of $E_{\text{ph}} = 1.265 \text{ eV}$ (980-nm radiation), the applied- and zero-field

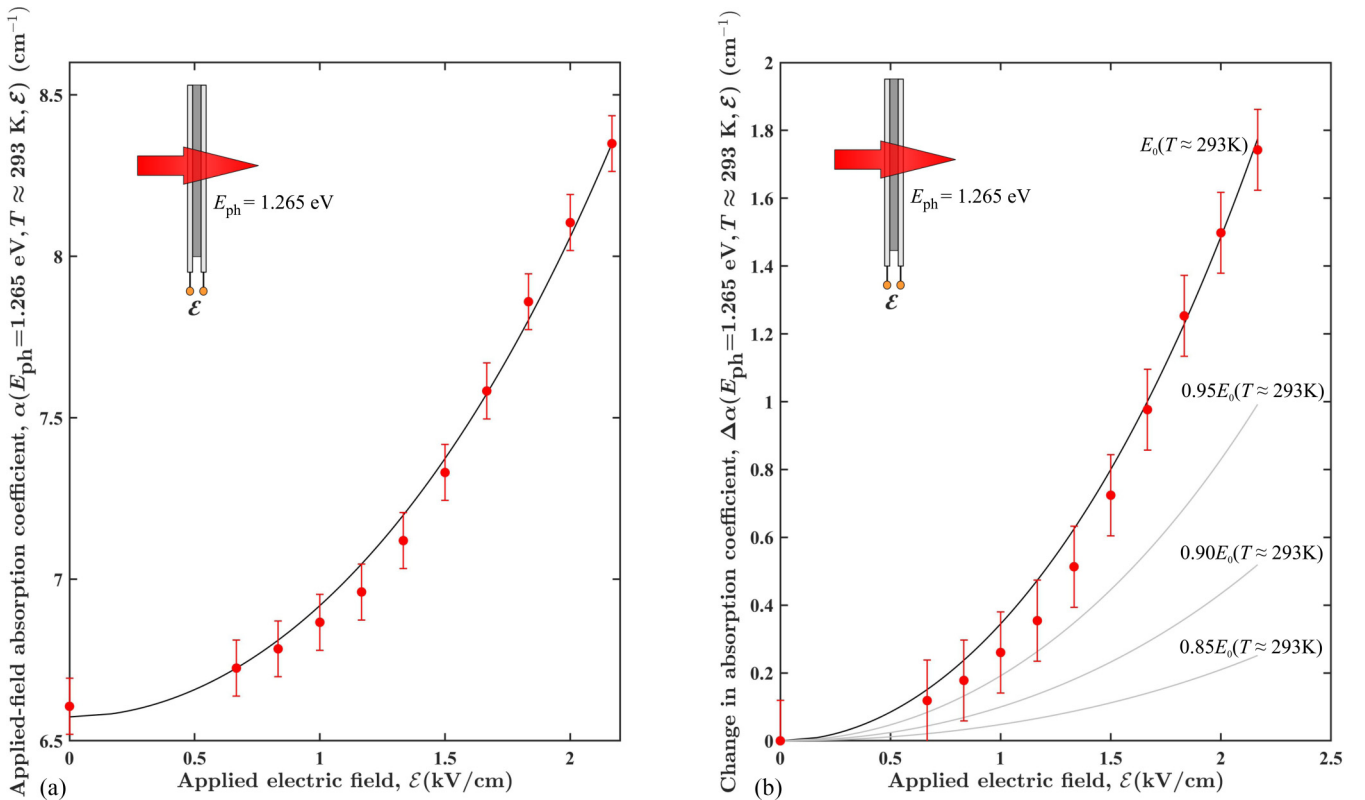


FIG. 3. The (a) applied-field absorption coefficient of SI-InP, $\alpha(E_{\text{ph}} = 1.265 \text{ eV}, T \approx 293 \text{ K}, \mathcal{E})$, at a photon energy of $E_{\text{ph}} = 1.265 \text{ eV}$ (980 nm radiation) and room temperature, $T \approx 293 \text{ K}$, as a function of applied electric field \mathcal{E} and the (b) change in absorption coefficient of SI-InP, $\Delta\alpha(E_{\text{ph}} = 1.265 \text{ eV}, T \approx 293 \text{ K}, \mathcal{E})$, at a photon energy of $E_{\text{ph}} = 1.265 \text{ eV}$ (980 nm radiation) and room temperature, $T \approx 293 \text{ K}$, as a function of applied electric field \mathcal{E} . The results are displayed as experimental (red) markers and fitted theoretical (black / grey) curves: black curves denote the characteristic width of $E_0(T \approx 293 \text{ K})$; grey curves denote characteristic widths reduced to $0.95 E_0(T \approx 293 \text{ K})$, $0.90 E_0(T \approx 293 \text{ K})$, and $0.85 E_0(T \approx 293 \text{ K})$.

absorption coefficients are $\alpha(E_{\text{ph}} = 1.265 \text{ eV}, T \approx 293 \text{ K}, \mathcal{E} = 2.17 \text{ kV/cm}) = 8.35 \text{ cm}^{-1}$ and $\alpha(E_{\text{ph}} = 1.265 \text{ eV}, T \approx 293 \text{ K}, \mathcal{E} = 0 \text{ kV/cm}) = 6.61 \text{ cm}^{-1}$, respectively, with the change in absorption coefficient, $\Delta\alpha(E_{\text{ph}} = 1.265 \text{ eV}, T \approx 293 \text{ K}, \mathcal{E} = 2.17 \text{ kV/cm}) = 1.74 \text{ cm}^{-1}$, depending on the applied electric field, as detailed next.

Figure 3(a) shows results for the applied-field absorption coefficient of SI-InP, $\alpha(E_{\text{ph}} = 1.265 \text{ eV}, T \approx 293 \text{ K}, \mathcal{E})$, at a photon energy of $E_{\text{ph}} = 1.265 \text{ eV}$ (980 nm radiation) and room temperature, $T \approx 293 \text{ K}$, as a function of applied electric field \mathcal{E} . The results are displayed as experimental (red) markers and fitted theoretical (black) curves. The absorption coefficient rises for increasing field, as expected, with good agreement between the measured data and fitted curves for the fitting parameter defined above. Through these analyses, we found that the temperature was raised slightly as the field increased, and it was necessary to include the temperature dependence to obtain a precise fit. This dependence is discussed in the following section. More importantly, we find that the above trends could not be realized without considering the continuum of Urbach tail states into the band gap and their manifestation in the Einstein model.

Figure 3(b) illustrates the role of the Einstein model by showing results for the applied-field absorption coefficient, $\alpha(E_{\text{ph}} = 1.265 \text{ eV}, T \approx 293 \text{ K}, \mathcal{E})$, at a photon energy of $E_{\text{ph}} = 1.265 \text{ eV}$ (980nm radiation) and room tempera-

ture, $T \approx 293 \text{ K}$, as a function of applied electric field \mathcal{E} . The results are shown as experimental (red) markers and fitted theoretical (black) curves at a characteristic width, $E_0(T \approx 293 \text{ K})$, scaled by 1.0, 0.95, 0.90, and 0.85. We see here that the Urbach tail states encroaching into the band gap play a critical role in absorption. For example, at an applied electric field of $\mathcal{E} = 2.17 \text{ kV/cm}$, we see relatively small reductions of the characteristic width, by 0, 5, 10, and 15%, which greatly reduce the absorption coefficient, by 0, 47, 74, and 88%, respectively.

V. DISCUSSION

The experimental and theoretical results in the preceding section show good agreement for the field-induced absorption of SI-InP, with dependencies on photon energy, temperature, and electric field that are well explained by the unified Franz-Keldysh and Einstein model. Nonetheless, the experimental results do show some deviations from the theoretical results, largely in Fig. 3, and these are worthy of discussion.

The deviations seen between the experimental and theoretical results could potentially be attributed to the ignoring of Coulomb (exciton) interaction in our unified model, which only considers the density of states (Urbach tail) distribution. With this in mind, we have used the control parameters δ_{CB}

and δ_{VB} to truncate the integral limits in Eq. (6) and explored the contributions from energy states within and above the band gap. In doing this, we found that the greatest contributions from the density of states (Urbach tail) distribution arise from energy states near the photon energy, E_{ph} . This suggests that the significant damping at these energy states from the exponential function in the integrand is outweighed by stronger growth of the neighboring $\alpha_i(E, E_{ph}, \mathcal{E})$ function, due to the small separation between E and E_{ph} in the Franz-Keldysh effect. In contrast, contributions from the Coulomb (exciton) interaction arise from energy states near the conduction and valence band edges. These contributions manifest as a linear trend in absorption coefficient versus energy, within roughly 10 meV of the band-gap energy, which transitions to the above-defined exponential function at energy states further from the band-gap energy [15]. (Note that these contributions also modify the density of states, and thus the absorption above the band-gap energy). Given the narrow range of energies over which Coulomb (exciton) interaction manifests, within 10 meV of the band-gap energy, $E_g(T \approx 293 \text{ K}) = 1.352 \text{ eV}$, we believe that this interaction will be weak at the photon energies of our work, $E_{ph} = 1.24\text{--}1.30 \text{ eV}$. Moreover, the interaction would be nondispersive, i.e., independent of photon energy, and so its effects would be encompassed in our multiplicative fitting parameter.

The deviations seen between the experimental and theoretical results could also potentially be attributed to the accuracy of the (simple) Einstein model in characterizing the band edge. With this in mind, we have repeated the fitting in this work with the (more common) Varshni model, as it often shows better agreement between experimental and theoretical results [13,16]. The Varshni model is a simple empirical relation that assumes an average phonon energy, and so it is best used with semiconductors exhibiting little phonon dispersion at temperatures above 100 K [17]. In comparing the fitting, we found that the Einstein and Varshni models yield similar root-mean-square percentage errors for Fig. 3(a), at 0.6% and 1.3%, respectively, and Fig. 3(b), at 8.8% and 9.2%, respectively. Thus, the Varshni model, while accurate for others, does not lessen the deviations seen between the experimental and theoretical results.

Ultimately, we believe the deviations seen between the experimental and theoretical results can be attributed to an observed dependence of the SI-InP temperature T on the applied electric field \mathcal{E} . We used a Taylor series expansion to characterize this dependence of T on \mathcal{E} , with constant coefficients in the terms populated by fitting. The fitting gave negligible first-order and third-order terms, with the remaining (constant) zeroth-order and second-order terms showing a temperature increase in proportion to the applied electric power, i.e., electric field squared. Such a finding is physically sound, as it conveys power conservation. When we incorporated this field-dependent temperature into our model, as $T \approx 293 \text{ K} + [0.647 \text{ K} (\text{kV}/\text{cm})^{-2}] \mathcal{E}^2$, we found that it greatly improved the fit between the experimental and theoretical results, even though the field-induced increases in temperature were small (at less than 3 K). It also became evident that the coefficient of the second-order term scaled with the incident optical power. Such a finding is physically sound, given that the high resistivity of SI-InP ($10^8 \Omega \text{ cm}$) cannot sustain cur-

rent. The incident optical power is needed to generate charge carriers, conduction current, and Joule heating.

In characterizing the dynamics of temperature, we found that its dependence on the applied electric field and Franz-Keldysh effect together could lead to fluctuations in the absorption coefficient about metastable states. According to the Franz-Keldysh effect, an increasing electric field increases the absorption coefficient and absorbed optical power, which increases the temperature. The increased temperature then further increases the absorption coefficient and temperature—with the cycle continuing towards a metastable state. We observed the effects of such fluctuations about metastable states within the experimental results, with the greatest effects seen at high optical powers and applied electric fields. As such, we set the optical power and applied electric fields to values that balance our desires for relatively weak metastability and fluctuations (at sufficiently low powers and fields) and for relatively strong signals (at sufficiently high powers and fields). The effects of metastability were then encompassed into the model via the above T versus \mathcal{E} expression and the remaining fluctuations were portrayed by error bars in the figures. Such a procedure gave a good fit between the experimental and theoretical results with an accurate understanding of the remaining deviations.

VI. CONCLUSION

In this work, we applied the foundational Franz-Keldysh and Einstein models to characterize semiconductor band-edge absorption—and its departures from ideality. Our unified model characterized absorption under field-induced tunneling of photoexcited electrons from degenerate heavy- and light-hole valence bands to the conduction band, with encroachment into the band gap in the form of an Urbach tail. The theoretical results showed strong agreement with our experimental results, for SI-InP, under a wide range of photon energies, temperatures, and electric fields. Such findings suggest that the Urbach tail and its manifestation via the Einstein model can be important in characterizing the field-induced changes in absorption brought about by the Franz-Keldysh effect.

It is hoped that the proposed work will give deeper insight on light and field interactions within semiconductors and their growing application to electroabsorption modulators. Electroabsorption modulators are often implemented with multi-quantum-well layers [18–20] to establish band edges with energies slightly above the photon energy and yield appreciable modulation depths. Nonetheless, there is a desire to implement electroabsorption modulators with existing laser wavelengths and nonepitaxial semiconductors [21,22]. The combination of a 980-nm laser (having $E_{ph} = 1.265 \text{ eV}$) and SI-InP (having $E_g(T \approx 293 \text{ K}) = 1.352 \text{ eV}$) suggests that this is possible. While the separation between these energies, 87 meV, would be considered too large to overcome according to the idealized Franz-Keldysh effect, our work shows that the Urbach tail states encroaching into the band gap can bring about the desired strong electroabsorption. The unified Franz-Keldysh and Einstein models support this interpretation and effectively characterize the dependencies on photon energy, temperature, and electric field.

ACKNOWLEDGMENTS

This research was funded by the Natural Sciences and Engineering Research Council of Canada, Grant No. RGPIN-2017-04073, the Canada Foundation for Innovation, Grant No. LOF 16659, and Western Economic Diversification Canada.

APPENDIX

The two integral functions defined in Eq. (7) can be integrated using the identities in [23] and computed for each integer j via recursion relations. The $I_j(z_i)$ function and its recursion relations are defined by

$$I_j(z_i) = \int z_i^j \text{Ai}^2(z_i) dz_i, \quad (\text{A1})$$

$$I_1(z_i) = (1/3)[\text{Ai}'(z_i)\text{Ai}(z_i) - z_i \text{Ai}^2(z_i) + z_i^2 \text{Ai}^2(z_i)], \quad (\text{A2})$$

$$I_2(z_i) = (1/5)[2z_i \text{Ai}'(z_i)\text{Ai}(z_i) - \text{Ai}^2(z_i) - z_i^2 \text{Ai}^2(z_i) + z_i^3 \text{Ai}^2(z_i)], \quad (\text{A3})$$

$$I_3(z_i) = (1/7)[3z_i^2 \text{Ai}'(z_i)\text{Ai}(z_i) - 3\text{Ai}^2(z_i) - z_i^3 \text{Ai}^2(z_i) + z_i^4 \text{Ai}^2(z_i)], \quad (\text{A4})$$

$$I_{j>3}(z_i) = [1/(2j+1)]\{jz_i^{j-1} \text{Ai}'(z_i)\text{Ai}(z_i) - j(j-1)[z_i^{j-2} \text{Ai}^2(z_i) - (j-2)I_{j-3}(z_i)]/2 - z_i^j \text{Ai}^2(z_i) + z_i^{j+1} \text{Ai}^2(z_i)\}. \quad (\text{A5})$$

The $H_j(z_i)$ function and its recursion relations are defined by

$$H_j(z_i) = \int z_i^j \text{Ai}'(z_i)^2 dz_i, \quad (\text{A6})$$

$$H_0(z_i) = (1/3)[2\text{Ai}'(z_i)\text{Ai}(z_i) + z_i \text{Ai}^2(z_i) - z_i^2 \text{Ai}^2(z_i)], \quad (\text{A7})$$

$$H_1(z_i) = (1/5)[3z_i \text{Ai}'(z_i)\text{Ai}(z_i) - 3\text{Ai}^2(z_i)/2 + z_i^2 \text{Ai}^2(z_i) - z_i^3 \text{Ai}^2(z_i)], \quad (\text{A8})$$

$$H_2(z_i) = (1/7)[4z_i^2 \text{Ai}'(z_i)\text{Ai}(z_i) - 4\text{Ai}^2(z_i) + z_i^3 \text{Ai}^2(z_i) - z_i^4 \text{Ai}^2(z_i)], \quad (\text{A9})$$

$$H_{j>2}(z_i) = [1/(2j+3)]\{(j+2)z_i^j \text{Ai}'(z_i)\text{Ai}(z_i) - j(j+2)[z_i^{j-1} \text{Ai}^2(z_i) - (j-1)I_{j-2}(z_i)]/2 + z_i^{j+1} \text{Ai}^2(z_i) - z_i^{j+2} \text{Ai}^2(z_i)\}. \quad (\text{A10})$$

-
- [1] W. Franz, Einfluß eines elektrischen felde auf eine optische absorptionskante, *Z. Naturforsch* **13**, 484 (1958).
- [2] L. V. Keldysh, The effect of a strong electric field on the optical properties of insulating crystals, *Zh. Eksp. Teor. Fiz.* **34**, 1138 (1958) [*Sov. Phys. JETP* **7**, 788 (1958)].
- [3] B. R. Bennett and R. A. Soref, Electrorefraction and electroabsorption in InP, GaAs, GaSb, InAs, and InSb, *IEEE J. Quantum Electron.* **23**, 2159 (1987).
- [4] J. K. Wahlstrand and J. E. Sipe, Independent-particle theory of the Franz-Keldysh effect including interband coupling: Application to calculation of electroabsorption in GaAs, *Phys. Rev. B* **82**, 075206 (2010).
- [5] B. O. Seraphin and N. Bottka, Electric field on the refractive index in GaAs, *Appl. Phys. Lett.* **6**, 134 (1965).
- [6] P. Pintus, Z. Zhang, S. Pinna, M. A. Tran, A. Jain, M. J. Kennedy, L. Ranzani, M. Soltani, and J. E. Bowers, Characterization of heterogeneous InP-on-Si optical modulators operating between 77 K and room temperature, *APL Photonics* **4**, 100805 (2019).
- [7] M. Chester and P. H. Wendland, Electroabsorption Spectrum in Silicon, *Phys. Rev. Lett.* **13**, 193 (1964).
- [8] I. R. Hristovski, N. I. Lesack, L. A. Herman, and J. F. Holzman, Urbach-edge-assisted electro-absorption for enhanced free-space optical modulation, *Opt. Lett.* **45**, 2478 (2020).
- [9] D. Redfield, Effect of defect fields on the optical absorption edge, *Phys. Rev.* **130**, 916 (1963).
- [10] F. Duque-Gomez and J. E. Sipe, The Franz-Keldysh effect revisited: Electroabsorption including interband coupling and excitonic effects, *J. Phys. Chem. Solids* **76**, 138 (2015).
- [11] K. Prosyk, M. Boudreau, and M. Scheer, Band tail modeling of bulk InGaAsP, *IEEE Photon. Technol. Lett.* **19**, 242 (2007).
- [12] M. Beaudoin, S. R. Johnson, A. J. G. DeVries, A. Mohades-Kassai, and T. Tiedje, Temperature dependence of the optical absorption edge in indium phosphide, *Mater. Res. Soc. Symp. Proc.* **421**, 367 (1996).
- [13] M. Beaudoin, A. J. G. DeVries, S. R. Johnson, H. Laman, and T. Tiedje, Optical absorption edge of semi-insulating GaAs and InP at high temperatures, *Appl. Phys. Lett.* **70**, 3540 (1997).
- [14] X. Wang, D. Yu, and S. Xu, Determination of absorption coefficients and Urbach tail depth of ZnO below the bandgap with two-photon photoluminescence, *Opt. Express* **28**, 13817 (2020).
- [15] I. Galbraith and B. Ryvkin, Empirical determination of the electroabsorption coefficient in semiconductors, *J. Appl. Phys.* **74**, 4145 (1993).
- [16] A. A. Humayun, A. Z. Alam, S. Khan, M. F. A. Malek, and M. A. Rashid, A comparative analysis of the effect of temperature on band-gap energy of gallium nitride and its stability beyond room temperature using Bose-Einstein model and Varshni's model, *IIUM Eng. J.* **18**, 151 (2017).
- [17] L. Gupta, S. Rath, S. Abbi, and F. Jain, Temperature dependence of the fundamental band gap parameters in cadmium-rich $\text{Zn}_x\text{Cd}_{1-x}\text{Se}$ using photoluminescence spectroscopy, *Pramana J. Phys.* **61**, 729 (2003).
- [18] J. Gao, J. Sun, J. Jiang, and Y. Zhang, Demonstration of biaxially tensile-strained Ge/SiGe multiple quantum well (MQW) electroabsorption modulators with low polarization dependence, *Nanophotonics* **9**, 4355 (2020).

- [19] Z. Chen, Z. Ikonic, D. Indjin, and R. W. Kelsall, Design considerations of intra-step SiGeSn/GeSn quantum well electroabsorption modulators, *J. Appl. Phys.* **130**, 153103 (2021).
- [20] M. Akie, T. Fujisawa, T. Sato, M. Arai, and K. Saitoh, GeSn/SiGeSn Multiple-quantum-well electroabsorption modulator with taper coupler for mid-infrared Ge-on-Si platform, *IEEE J. Sel. Top. Quantum Electron.* **24**, 3400208 (2018).
- [21] J. Verbist, M. Verplaetse, S. A. Srinivasan, J. Van Kerrebrouck, P. D. Heyn, P. Absil, T. D. Keulenaer, R. Pierco, A. Vyncke, G. Torfs, X. Yin, G. Roelkens, J. Van Campenhout, and J. Bauwelinck, Real-time 100 Gb/s NRZ and EDB transmission with a GeSi electroabsorption modulator for short-reach optical interconnects, *J. Light. Technol.* **36**, 90 (2018).
- [22] A. Abbasi, B. Moeneclaey, J. Verbist, X. Yin, J. Bauwelinck, G. Duan, G. Roelkens, and G. Morthier, Direct and electroabsorption modulation of a III-V-on-silicon DFB laser at 56 Gb/s, *IEEE J. Sel. Top. Quantum Electron.* **23**, 1501307 (2017).
- [23] J. R. Albright, Integrals of products of Airy functions, *J. Phys. A: Math. Gen.* **10**, 485 (1977).